HHS Public Access

Author manuscript

ACS Appl Mater Interfaces. Author manuscript; available in PMC 2021 July 28.

Published in final edited form as:

ACS Appl Mater Interfaces. 2021 May 12; 13(18): 20947–20959. doi:10.1021/acsami.0c21868.

Dynamic Tuning of Viscoelastic Hydrogels with Carbonyl Iron Microparticles Reveals the Rapid Response of Cells to Three-Dimensional Substrate Mechanics

Kiet A. Tran[1], **Emile Kraus**[2], **Andy T. Clark**[3], **Alex Bennett**[4], **Katarzyna Pogoda**[5], **Xuemei Cheng**[3], **Andrejs Cēbers**[6], **Paul A. Janmey**[7], **Peter A. Galie**[1]

[1.]Department of Biomedical Engineering, Rowan University, Glassboro, NJ, USA. [2.]Department of Physics and Astronomy, University of Pennsylvania, Philadelphia, PA, USA. [3.]Department of Physics, Bryn Mawr College, Bryn Mawr, PA, USA [4.]Department of Mechanical Engineering and Applied Mechanics, University of Pennsylvania, Philadelphia, PA, USA. [5.]Department of Experimental Physics of Complex Systems, Institute of Nuclear Physics, Polish Academy of Sciences, PL-31342, Krakow, Poland [6.]Department of Physics, University of Latvia, Riga, Latvia [7.]Department of Physiology, University of Pennsylvania, Philadelphia, PA, USA

Abstract

Current methods to dynamically tune three-dimensional hydrogel mechanics require specific chemistries and substrates that make modest, slow, and often irreversible changes to their mechanical properties, exclude the use of protein-based scaffolds, or alter hydrogel microstructure and pore size. Here, we rapidly and reversibly alter the mechanical properties of hydrogels consisting of extracellular matrix proteins and proteoglycans by adding carbonyl iron microparticles (MP) and applying external magnetic fields. This approach drastically alters hydrogel mechanics: rheology reveals that application of a 4,000 Oe magnetic field to a 5 mg/mL collagen hydrogel containing 10 wt% MPs increases the storage modulus from approximately 1.5 kPa to 30 kPa. Cell morphology experiments show that cells embedded within these hydrogels rapidly sense the magnetically-induced changes to ECM stiffness. Ca^{2+} transients are altered within seconds of stiffening or subsequent softening, and slower but still dynamic changes occur in YAP nuclear translocation in response to time-dependent application of a magnetic field. The near instantaneous change in hydrogel mechanics provides new insight into the effect of changing extracellular stiffness on both acute and chronic changes in diverse cell types embedded in protein-based scaffolds. Due to its flexibility, this method is broadly applicable to future studies interrogating cell mechanotransduction in three-dimensional substrates.

Supporting Information

Magneto-rheology; high magnification confocal microscopy; scanning electron microscopy; immunofluorescence; human coronal arterial smooth muscle cells; cell morphology analysis; cell viability and quantification; COMSOL simulation; magnetic flux density measurements.

Keywords

Biomaterials – Cells; Materials Science; Cell Mechanobiology; Physical Science; Biotechnology – Microparticles; Extracellular Matrix (ECM) Mechanics

1. Introduction

Our understanding of how cells respond to the mechanics of their extracellular matrix (ECM) has been traditionally informed by experiments using two-dimensional (2D) substrates[1,2]. These studies have demonstrated that cells alter their morphology[3], signaling[4], and phenotype[5] based on the mechanical properties of polyacrylamide or polydimethylsiloxane substrates to which they are attached. Yet, most non-epithelial cell types are fully surrounded by their ECM, and 2D substrates are unable to capture this aspect of the in vivo microenvironment. Alternatively, cells can be seeded within three-dimensional (3D) hydrogels to mimic cell-ECM interactions. Studies using hydrogels have identified multiple facets of the cell response that differ between 2D and 3D geometries[6,7]. However, in contrast to the linearly elastic substrates used for 2D mechanotransduction studies, the mechanics of 3D hydrogels, especially those comprised of natural proteins including collagen and fibrin, are complicated by viscoelastic and strain stiffening properties that have been shown to alter the cell response[8–11]. Nonetheless, these properties are more representative of the mechanics of the ECM in vivo.

Although 3D hydrogels better mimic the geometry and mechanics of the ECM, tuning the mechanical properties of these scaffolds is more difficult than 2D substrates. Doing so dynamically is even more challenging. Currently, methods to alter the mechanics of cell-seeded 3D scaffolds rely primarily on photocrosslinkable[12,13] and photodegradable[14,15] chemistries. However, these approaches generally require substantial modification of hydrogel chemistry and composition and cannot be reversibly cycled through a broad range of mechanical properties. Moreover, cytotoxicity assays reveal that cell viability significantly decreases as the concentration of photocrosslinkers increases, limiting the possible range over which these substrates can be tuned. Studies have found that altering the degradability of these hydrogels affects the cell response to the mechanics of their surroundings, preventing direct interrogation of the effect of 3D substrate stiffness[12]. These limitations necessitate a reversible and repeatable method to modify hydrogel mechanics without changing the microstructure of the surrounding fibrous matrix.

Magnetorheological materials containing carbonyl iron microparticles (MPs) provide a means to overcome the limitations of previous methods to tune hydrogel mechanics. These materials respond to external magnetic fields in a rapid, reversible, and repeatable manner[16,17]; their stiffness can substantially increase or decrease by changing the strength of the magnetic field. This effect is dependent upon MP concentration, demonstrating that greater changes can be achieved by adding more magnetic particles[18]. Previous studies have used 2D substrates embedded with MPs to study cell mechanotransduction[16]. However, cells can also be embedded inside of magnetorheological materials like kappa-carrageenan and N, N-dimethylacrylamide (DMAAm) and laponite without a loss of viability[19,20].

This study evaluates the ability of MPs to dynamically tune the mechanical properties of hydrogels consisting of natural proteins and proteoglycans, creating a method that is applicable to a broader range of scaffolds than previously described synthetic magnetorheological materials. Here, scaffold mechanics are dynamically tuned by submerging carbonyl iron MPs and applying an external magnetic field. Embedding 10 wt% MPs into a 5 mg/mL collagen scaffold with the application of 4,000 Oe magnetic field drastically increases the storage modulus from approximately 1.5 kPa to 30 kPa. More importantly, translating this approach to hydrogels containing proteins and proteoglycans gives rise to a more physiologically-relevant platform to control cell morphology, mechanosensing pathways, and calcium transients. The findings described in this study demonstrate that magnetically-responsive hydrogels provide a new means to rapidly and reversibly tune hydrogel mechanics to evaluate cellular mechanotransduction in 3D.

2. Experimental Section

2.1. Hydrogel preparation

Magnetic-responsive (MR) hydrogels were constructed by seeding carbonyl iron microparticles (MPs) into hydrogels prior to polymerization. Hydrogels either consisted of collagen, fibrin, or a mixture of collagen and high molecular weight (2–2.4 MDa) hyaluronan. Collagen hydrogels were fabricated using a previous method at concentrations of either 2 or 5-mg/mL[21,22]. 1 mg/mL fibrin hydrogels were polymerized using 1U/mL of thrombin. Hyaluronan was added to the collagen gels without any additional crosslinking. The collagen and collagen/HA concentrations were chosen to match previous studies of astrocyte-seeded hydrogels[23]. MPs were sterilized with 70% ethanol, dried by evaporation, and subsequently submerged in distilled water at a stock concentration of 100 wt% (w/v) 24 hours prior to hydrogel preparation.

2.2 Scanning electron microscopy (SEM)

Carbonyl iron microparticle were seeded into 5 mg/mL collagen hydrogels with a concentration of 0.1 wt% for matrix characterization. Hydrogels were thoroughly washed and fixed with 5% glutaraldehyde (VWR) for 30 minutes at 4°C. Following fixation, MR-gels were rinsed with PBS and sequentially dehydrated in 20%, 50%, 70%, 90% and 100% ethanol (VWR) for 10 minutes at room temperature. These samples were lyophilized for 2 hours and sputter coated prior to SEM imaging.

2.3. Mechanical characterization

Rheology measurements of collagen-based hydrogels were conducted on a magnetorheometer attachment for a TA Discovery rheometer (TA Instruments). MR collagen hydrogels were deposited directly onto the 37°C surface plate of the rheometer after mixing. A nonferrous 20-mm Peltier plate was set to a gap height of 00 μm. 1% cyclic strain at a frequency of 1 Hz was applied to the MR gels for a total time of 900 s, with no magnetic field applied during the first 300 s. Magnetorheological properties were measured after hydrogel polymerization for the remaining 600 s. Each magnetic pulse was axially applied for 20 s, with an initial field strength of 500 Oersted (Oe), followed by 2000 Oe and then 4000 Oe. The storage and loss moduli were used to evaluate the tunable mechanical

properties of the magnetic-collagen hydrogels. In order to determine whether the direction of the field altered the rheological results, MR collagen hydrogels were polymerized on a non-ferrous Peltier plate (gap height: 24-μm) of a DHR-2 rheometer (TA Instrument) with a 1° 20-mm cone. The cyclic strain and frequency settings matched experiments using the magnetorheometer. A magnetic field of 500 Oe was applied in the transverse direction using permanent magnets. The rheology of fibrin- and PDMS-based materials was measured with an Anton Paar rheometer (MCR502, Anton Paar GmbH, Germany) equipped with a temperature-controlled electromagnet that produces a uniform field perpendicular to the face of a disk-shaped samples between parallel plates. The sample diameter was 20 mm and height varied from 0.3 to 1 mm. Shear storage and loss moduli (G' and G", respectively) were measured as a function of magnetic field at 1% shear strain a frequency of 10 rad/s.

In order to visualize MP displacement within fibrin hydrogels, unpolymerized hydrogels were added to a transparent stage and a 20-mm flat disk applied controlled levels of shear stress using a Bohlin rheometer. For these experiments, a constant magnetic field of 1000 Oe was applied horizontally across the disk-shaped hydrogel using permanent magnets. The instantaneous MP deformation was tracked during the initial application of shear stress, and then tracked during the creep period while the rheometer tracked creep angle.

2.4. Confocal Microscopy

Confocal microscopy was used to examine whether the application of the magnetic field caused carbonyl iron MP displacement. For these experiments, 1 wt% of Nile-red magnetic MPs were embedded in 2 mg/mL and 5 mg/mL collagen hydrogels. After suspending the MPs, gels were either immediately transferred to the stage of a Nikon A1 laser scanning confocal microscope or incubated for an hour to polymerize. Images were taken with a 40X oil immersion objective (Nikon) to visualize displacement over a total period of 40-s. The gels were unmagnetized for the first 20-s and a magnetic field of 2700 Oe was applied to the gel for an addition 20-s for all conditions.

2.5. Microfabricated devices

Cell-seeded collagen hydrogels were polymerized inside a polydimethylsiloxane (PDMS)-based device fabricated using soft lithography[24,25]. Briefly, a rectangular chamber was fabricated using positive-feature PDMS stamps with dimensions of 4 mm × 6 mm × 2 mm (L × W × H). The feature layers were cured at 150°C for 7 mins. The top of these devices remained open to allow nutrient and oxygen transport. In addition to nutrient transport, we found that adding 3-mm glass spacers on each side of these devices substantially increased cell viability.

2.6. Cell Culture

Human coronary artery smooth muscle cells (hCASMC) infected with RFP-LifeAct using an MOI were thawed at passage 6 and cultured in smooth muscle cell growth medium (Lonza) until confluency. P5 normal human astrocytes (NHA) were cultured in astrocyte growth medium (AGM, Lonza) according to a previous protocol[26].

2.7. Live cell microscopy of hCASMC-mediated bead displacement

Cells were seeded into MR collagen-hyaluronan composite hydrogels at a cell density of 1×10^6 cells/mL. A particle concentration of 0.5 wt% was chosen to visualize local deformation mediated by hCASMCs. Following suspension, the collagen-cell solution was injected into the central chamber of the microfabricated device and placed in a tissue plastic 35 mm petri dish that contained 5 mL of SMC growth medium. These hydrogels were incubated for 15 min and transferred to a live-cell incubator (Nikon). For gels exposed to a magnetic field, four neodymium magnets (two N52 magnets on each side, 1.5” x 0.5” x 0.125”, BX882-N52, K&J Magnetics) were positioned to apply a horizontally-oriented 500-Oe magnetic field to the hydrogels. Encapsulated cells were imaged using an inverted epi-fluorescent microscope (Nikon) for 3 hours. These images were then analyzed using FIJI and MATLAB.

2.8. Cell viability assays

To examine the effect of MP concentration on astrocyte viability, P5 normal human astrocytes (NHAs) were seeded at a density of 1×10^6 cells/mL into 5-mg/mL collagen hydrogels with the following MP concentrations: 0 wt%, 0.5 wt%, 2.5 wt%, 5 wt%, 10 wt%, and 20 wt%. After 3 days, cell-seeded hydrogels were washed twice with PBS and stained with 4 mM of calcein AM and 2 mM of EthD-III (Biotium) for 45 minutes at room temperature. Hydrogels were imaged on a Nikon A1 laser scanning confocal microscope. Five frames were used for each condition to quantify cell viability.

2.9. Cell morphology and mechanotransduction studies of normal human astrocytes

Similarly, NHAs were seeded into MR collagen hydrogels at a density of 1×10^6 cells/mL. A magnetic particle concentration of 5 wt% was used to increase the effect of the magnetic field on substrate stiffness. The collagen-cell solution was injected into the central chamber of the microfabricated devices, placed in a P100 tissue plastic petri dish, and incubated for 15 minutes. For gels exposed to a magnetic field, eight neodymium magnets (four N52 magnets on top and underneath, 1.5” x 0.5” x 0.125”, BX882-N52, K&J Magnetics) were positioned with 2-mm spacers to apply a vertically-oriented 7,700-Oe magnetic field. A computational model constructed in COMSOL was used to calculate the magnitude and uniformity of the field in the region of the hydrogels (Figure S1A-C). In order to construct the model, a gauss meter (Model 410, LakeShore) was used to measure the surface field of a single BX882-N52 magnet and at locations 2- and 4-mm removed from the surface. The Br parameter in COMSOL was set at 1.145 to produce the correct surface field (1,780-Oe) (Figure S1D). The measurements of the gauss meter at 2- and 4-mm from the surface showed good agreement with the computational results (Figure S1E). The COMSOL model predicted a field of approximately 7,200-Oe, which was close to the 7,700-Oe field measured by the gauss meter. For negative controls, the same NHA density was seeded into hydrogels without magnetic particles and also exposed to a 7,700-Oe magnetic field. All cell-seeded hydrogels were incubated with AGM throughout the experiment.

2.10. Immunocytochemistry

For immunocytochemical staining, culture medium was aspirated from the gels followed by PBS wash and fixation in 4% paraformaldehyde (Alfa Aesar) at room temperature for 30 min. Gels were then permeabilized with 0.2% Triton X-100 (Sigma) for 30 min at room temperature. MR collagen hydrogels were removed from the central chamber and blocked with 3% bovine serum albumin (BSA) for 30 min at room temperature. The permeabilized hydrogels were incubated with 1:200 yes-associated protein (YAP) primary antibodies overnight at 4°C. These gels were then washed thoroughly with PBS and incubated with 1:250 DAPI, 1:50 TRITC phalloidin, and 1:200 secondary antibody 488 at 37°C for 60 min. Images were acquired on a Nikon A1 laser scanning confocal microscope.

2.11. Calcium transient measurements in hCASMC-seeded hydrogels

To examine the effect of rapidly changing matrix mechanics on cell response, LifeAct-transfected hCASMC were seeded into 2 mg/mL collagen with and without 2.5 wt% MPs at a density of 1×10^6 cells/mL. The cell-seeded hydrogels were incubated at 37°C with smooth muscle cell growth media 24h prior to imaging to preserve optimal spreading. To observe calcium transients in real time, SMCs were incubated with 20 μM Fluo-4 AM (Life Technologies) in DMEM/F-12 medium consisting of 10% FBS, 20 mM HEPES, and 0.25% pluronic acid for 45 minutes[27]. These hydrogels were then washed with F-12 media containing 10% FBS and 20 mM HEPES for 15 minutes and transferred to a live-cell incubator. Images were taken every 1-s for 9 minutes at a wavelength of 488-nm to visualize instantaneous calcium transients with respect to dynamically tuning the mechanical stiffness of the hydrogels. An external field of 2850 Oe was applied to the gels (indicated as “w/ MF”) for 3 minutes, removed for 3 minutes (“w/o MF”), and finally reapplied for the final 3 minutes of the experiment. Rheology indicated an increase in storage modulus from approximately 100 Pa to 650 Pa for these conditions. These experiments were conducted with and without magnetic particles to provide a negative control.

2.12. Image analysis

Spreading of NHAs was quantified using ImageJ. Z-stacks images of DAPI/phalloidin stained cells were taken with a laser scanning confocal microscope using a 40X oil immersion objective (Nikon) and condensed to create 2D images. For cell morphology measurements, the freehand selection tool was used to trace the area of the cell. Mean and standard deviations of these morphology measurements were then calculated. For measurements of cell shape index (CSI) and YAP nuclear localization in 3D, quantification was conducted as previously described[28]. Briefly, binary masks were generated for 3D image stacks of DAPI and actin images by using Otsu’s intensity-based thresholding method. The counter function was used to calculate cell volumes (V) and surface areas (A_0). The obtained values were used to calculate 3D CSI using the following equation: $CSI = \frac{\pi^{\frac{1}{3}}(6V)^{\frac{2}{3}}}{A_0}$[28]. The generated metric defined a line with a CSI of 0 and a sphere with a CSI of 1. For nuclear YAP localization measurements, single cell images were analyzed and quantified. Images were converted into binary masks to create thresholds for each color channel to determine nuclear volume (V_n) and cell cytoskeleton volume (V_c). The counter

function was again used to determine V_n and V_c along with the intensity of YAP signal within those regions. The measured values were inserted into the following equation to generate YAP nuclear/cytosolic ratio: $Nuclear\ YAP = \frac{\frac{Nuclear\ YAP\ signal}{V_n}}{\frac{Cytosolic\ YAP\ signal}{V_c}}$[28]. In order to quantify calcium transients, fluorescent intensities inside of each cell were measured for individual frames during the three phases of the hydrogels. Normalized Fluo-4 fluorescence ratios were expressed as $(F\text{-}F_0)/(F_{max}\text{-}F_0)$ (instantaneous fluorescence – initial fluorescence/ maximum fluorescence - initial fluorescence) to compare differences in calcium cycling. Transients were averaged for each condition, and the initial slope of the transient was measured by fitting a line to the increase in normalized fluorescence.

2.13. Statistical analysis

Two-sample t-tests, One-way ANOVA, two-way ANOVA, and post-hoc Tukey's HSD tests were used to calculate statistical significance. Statistical significance of the rheological MP deformation was calculated using a paired t-test, assuming normal distributions with unequal variances between groups. For morphology and YAP studies, measurements were averaged from at least 25 cells per condition.

3. Results

3.1. Magnetorheology of collagen and fibrin hydrogels seeded with magnetic particles

Initial experiments were used to quantify the effect of magnetic fields on the viscoelastic properties of collagen and fibrin hydrogels seeded with carbonyl iron MPs. Magnetic fields of increasing strengths were transiently applied to the hydrogels following polymerization within a cone-plate rheometer fitted with a coil to apply an axial magnetic field to the hydrogel (Figure 1A). To demonstrate the dynamic nature of this effect, 5 mg/mL collagen hydrogels were seeded with different concentrations of magnetic particles exposed to three increasing magnitudes of magnetic field for a duration of 20 seconds, with approximately 2 minutes in between application of the fields of 500 Oe, 2,000 Oe, and 4,000 Oe (Figure 1B). The storage and loss moduli are plotted as a function of time in Figures 1C-D. The largest increase in storage and loss modulus was observed in collagen hydrogels containing 10 wt% MPs and exposed to a 4,000 Oe magnetic field (Figure 1Ci,Di). The increase in storage modulus appeared to be proportional to the strength of the field for the range of conditions tested. Moreover, for all conditions, removing the magnetic field reversed the increase in viscoelastic properties, which is consistent with previous results[17]. Decreasing the concentration of magnetic particles reduced the effects of the magnetic field, although the increase remained proportional to the field strength. Next, the magnetic field was applied in the transverse direction to determine whether the direction of the field would alter the rheological measurements. Similar to the rheological tests on a magnetorheometer, a magnetic field of 500 Oe was transiently applied to 5-mg/mL collagen hydrogels seeded with 5 wt% and 10 wt% of MPs for a period of 20 seconds. The data demonstrated that the storage and loss modulus resulted in similar magnitudes as the measurements in the magnetorheometer, which applied a field in the axial direction (Figure S2). Increasing the magnitude of the magnetic field also resulted in an increase in the storage modulus of a 1

mg/mL fibrin hydrogel, as shown in Figure 1E, demonstrating the broad applicability of this approach. Overall, these results verify that previous observations of magnetoviscoelasticity in MR-composite gels[29,30] can be extended to protein-based hydrogels containing MPs.

3.2. Analytical model of magnetic-induced changes to hydrogel mechanics

An analytical model was used to provide a mechanistic basis to the rheological measurements, and MPs were seeded within a polydimethylsiloxane (PDMS) elastomer to validate the model. PDMS was chosen to test the theoretical model because, unlike collagen or fibrin, it is a nearly ideal linear, incompressible elastomer with a constant Poisson's ratio, affine deformation, and a very small mesh size that ensures no rotation or slippage of MPs when the field is applied or the sample is sheared. In the presence of a magnetic field, shear deformation of the gel causes the ferromagnetic MPs in the elastomer to become misaligned with the imposed field causing volume-distributed torques. The magnetic permeability of the gel becomes a function of the deformation tensor[31], u_{ik}. In Einstein summation notation:

$$\mu_{ik} = \mu^0 \delta_{ik} + a_1 u_{ik} + a_2 u_{ll} \delta_{ik} \quad \text{Equation (1)}$$

where μ^0 is the relative permeability of the undeformed gel, δ_{ik} is the Kronecker delta, and a_1 and a_2 are constants. Since the hydrogels are incompressible, $u_{ll} = 0$, and the last term can be omitted. The magnetic anti-symmetric stress, as in magnetic liquids, is

$$\sigma_{ik} = \frac{1}{2} \epsilon_{ikl} [\boldsymbol{M} \times \boldsymbol{H}_0]_l \quad \text{Equation (2)}$$

where ϵ_{ikl} is the Levi-Civita symbol, $\boldsymbol{M}$ is the magnetization, and $\boldsymbol{H_0}$ is the external magnetic field. Taking the z-direction to be the axial direction of the rheometer plate, the shear stress is then

$$\sigma_{xz} = \frac{1}{2} M_x H_z \quad \text{Equation (3)}$$

The deformation tensor for oscillatory rheometry can be modeled assuming linear shear

$$u_{xz} = \frac{1}{2} \frac{\partial u_x}{\partial z} \quad \text{Equation (4)}$$

The x-component of magnetization can be written as follows:

$$M_x = \frac{\mu_{xz}}{4\pi} H_z \quad \text{Equation (5)}$$

where μ_{xz} is the xz component of the magnetic permeability, and H_z is the z component of the internal magnetic field within the hydrogel taking the demagnetization into consideration. Writing μ_{xz} in terms of equation (1), and accounting for linear strain in (4) yields:

$$\mu_{xz} = a_1 u_{xz} = a_1\left(\frac{1}{2}\frac{\partial u_x}{\partial z}\right) \quad \text{6Equation (6)}$$

In the case of an incompressible gel, $H_z = \frac{H_0}{\mu^0}$, so the shear stress can be written as:

$$\sigma_{xz} = \frac{1}{16\pi} a_1 \left(\frac{H_0}{\mu^0}\right)^2 \frac{\partial u_x}{\partial z} \quad \text{Equation (7)}$$

using the value of a_1 from a previous experiment[32] and noting $\sigma_{xz} = G'\frac{\partial u_x}{\partial z}$, the shear modulus as a quadratic function of the external field is as follows:

$$G' = \frac{1}{40\pi}\frac{\left(\mu^0 - 1\right)^2}{\mu^0} H_0^2 \quad \text{Equation (8)}$$

From eq. 8, a plot of G' vs H was predicted to be quadratic in H, and the quantity μ^0 could be calculated from the fitting parameter. Experimentally, G' should have a finite value in the absence of a field due to the elastic properties of the elastomer in which the ferromagnetic particles are embedded. This value was treated as a constant in the fitting of the data. This theory was tested with 10 wt% MPs distributed homogenously in PDMS. As shown in Figure 1F, the increase in shear modulus was well fit by eq. 8, where $a = \frac{1}{40\pi}\frac{\left(\mu^0 - 1\right)^2}{\mu^0} = 6.88 \times 10^{-3}$. From this parameter, the magnetic permeability $\mu^0 = 2.5$ was in reasonable agreement with the value obtained from magnetometry measurements, $\mu^0_{exp} = 1.1$. Although the increasing rates were similar during the application of the magnetic field, the relative stiffening effect of the fibrin and collagen gels was much greater than in PDMS. Moreover, the increases in G' of fibrin and collagen were closer to linear than to quadratic in H. The reason for discrepancy with the theory is unknown but could be due to larger mesh sizes in these hydrogels compared to PDMS, the highly non-affine deformation of these networks in shear, or the non-linear elastic response of these fiber networks. Nevertheless, this model provides a mechanistic basis of the observed rheological results, and implies that the change in stiffness results from the intrinsic properties of the iron particles and not from an internal stress that they apply to the network in which they are embedded.

3.3. The effect of magnetic fields on magnetic particle displacement within hydrogels

A key assumption of the analytical model is that the magnetic particles are constrained within the network. In order to evaluate this assumption, fluorescently-labeled MPs were seeded within collagen hydrogels and observed by a resonance laser scanning confocal microscopy. Labeled MPs were tracked over a period of 20 seconds during the application of a magnetic field in collagen hydrogels of two different concentrations (2 and 5 mg/mL). In contrast to the rheology conducted in Figure 1, the magnetic field was applied perpendicular to the z-axis using permanent, neodymium magnets (the direction of the field is shown in

Figure S3) to allow higher resolution detection of small displacements. In order to assess the effect of fiber formation within the hydrogels, the MPs were tracked before and after polymerization. As Figure S3A-B indicates, a 2,500 Oe magnetic field caused measurable displacement of the MPs only before polymerization of the 2 mg/mL collagen gel. Once the hydrogel solidified, the magnetic field did not induce any measurable displacement of the particles. Figure S3C-D demonstrates a similar effect in the higher concentration collagen gel. Again, the magnetic field did not cause any measurable displacement in the polymerized hydrogel. The distribution of MP displacement over the 20-second period is graphed in Figure S3E-F for the 2 and 5-mg/mL hydrogels. Figure S3G shows that the collagen concentration had no significant effect on the total displacement of the MPs prior to polymerization. These findings indicate that the application of a magnetic field did not cause substantial displacement of the MPs in the polymerized collagen hydrogels even at the lowest concentration of collagen, indicating that the change in viscoelastic properties observed during magnetorheology was not caused by prestress on the fibrous network.

3.4. Tracking magnetic particle displacement within hydrogels under shear stress

In order to determine the effect of magnetic fields on the displacement of MPs in the presence of externally applied stress, a constant shear stress was applied by a flat plate rheometer fitted with a fluorescence microscope[33], so that MP displacement could be tracked during the initial application of stress and subsequent creep in the hydrogel (Figure 2A-B). These measurements were conducted at regions located at the same radial distance from the rotational axis for consistency. In order to demonstrate the broad applicability of this effect, these experiments used 1-mg/mL fibrin hydrogels containing 1 wt% fluorescently-labeled MPs. Figures 2C-E indicate the distribution of MP displacement with and without the presence of a 1,000 Oe field immediately following the application of 10, 25, and 50 Pa. These findings are consistent with previous studies that found a distribution of local strain within a fibrous network exposed to global strain[34]. For each magnitude of stress, the instantaneous MP displacement was substantially reduced in the presence of a magnetic field. The disparity was most apparent at the lowest level of applied stress (10 Pa). Not only did the magnetic field reduce the instantaneous displacement, but it also reduced the spread of the distribution, attenuating non-affine motion. To quantify this effect, the widths of the distributions at their half-heights were averaged across the three levels of stress and compared between magnetic and non-magnetic conditions (Figure 2F). The magnetic field also affected the creep behavior of the fibrin hydrogels. The creep rate was measured with two metrics: the deformation rate of the MPs as well as the creep angle recorded by the rheometer. Figure 2G shows that the magnetic field significantly decreased the deformation rate of the MPs at a stress of 50 Pa. These results are consistent with the creep rate measured by the rheometer plate for stress levels of 25 and 50 Pa plotted in Figure 2H. Overall, these results indicate that the magnetic field restricted the displacement of the MPs within hydrogels exposed to the external mechanical stimulus of shear stress, suggesting that the presence of the field reduces relative motion between MPs.

3.5. Cell-mediated magnetic particle displacement

Although rheological experiments revealed the effect of magnetic fields on MP displacement within a globally deformed fibrous network, this approach could not elucidate the effect of

magnetic fields on local deformation of MPs entrapped within the fibers. Therefore, live cell experiments were conducted by seeding 1×10^6 human coronary artery smooth muscle cells (hCASMCs) cells/mL into 5 mg/mL collagen and 1 mg/mL hyaluronan composite hydrogels containing 0.5 wt% MPs. The concentration of MP was chosen to visualize particle displacement in brightfield microscopy. A schematic of the microfabricated device containing the hydrogel is shown in Figure S4A. Additionally, a scanning electron microscopy image of the hydrogel containing 0.1 wt% MPs is shown in Figure S4B. Figure 3A provides a schematic of the cell-seeded hydrogels polymerized within a microfabricated device, and Figure 3B shows how the magnetic field was applied to the hydrogel while on the stage of an epifluorescence microscope using neodymium magnets. The magnets were positioned to apply a uniform field of 500 Oe to the cell-seeded hydrogels. This combination of magnetic field strength and MP density was chosen to increase hydrogel storage modulus without affecting the contractility of the smooth muscle cells: rheological results indicated that the application of a 500 Oe field to collagen hydrogels seeded with 0.5 wt% MPs increased the storage modulus by a modest amount (from 500 Pa to approximately 650 Pa). We found no significant difference between cell morphology and alpha-smooth muscle cell actin expression in the hCASMCs between this range of storage moduli (Figure S5), suggesting similar cell contractility in both conditions. Figure 3C shows a representative cell at 6-hrs post gel polymerization in the absence of a magnetic field. The displacement of the MPs in that time was quantified and displayed in the form of a heat map in Figure 3D. Both the cell and the displacement of adjacent MPs in the presence of a 500 Oe magnetic field are presented in Figure 3E. As the heat map indicates, the displacement of the MPs was substantially reduced in the presence of the magnetic field (Figure 3F). Quantification of total MP displacement distributions verified that application of the magnetic field reduced MP displacement (Figure 3G). Box plots provided in Figure 3H indicate a significant difference in MP displacement. These results are consistent with the rheological findings: the MPs are constrained from moving relative to one another in the presence of a magnetic field. Since the MPs are effectively trapped within the fibrous network, the magnetic field then increases the storage modulus of the hydrogel. This increase in stiffness was apparent in both global deformation (Figure 2) and local, cell-mediated matrix deformation (Figure 3).

3.6. Alteration of ECM mechanics instantaneously affects calcium transients

In order to highlight the ability of MR hydrogels to instantaneously change 3D substrate mechanics to an extent that alters the cell response, calcium transients were measured in smooth muscle cells seeded inside collagen hydrogels with and without MPs. 1×10^6 HCASMC/mL were seeded into 2-mg/mL collagen hydrogels without magnetic particles as negative controls. The same cell density was seeded into 2 mg/mL collagen hydrogels containing 2.5 wt% of MPs to observe the dynamic effects of magnetically induced stiffness changes on calcium transients. Application of a magnetic flux of 2850 Oe increased the storage modulus from approximately 100 Pa to 650 Pa (Figure S6), yielding a substantial increase in the stiffness of the hydrogel and providing an opportunity to interrogate how this change in stiffness altered calcium signaling. Spontaneous calcium transients were observed to occur at a frequency of approximately one cycle per three minutes in both MR and non-MP-seeded collagen hydrogels (Videos S1-2), so the magnetic field was applied for three

minutes (increased storage modulus), removed for the next three minutes (decrease storage modulus), and subsequently reapplied for three minutes (re-increase storage modulus).This "on-off-on" provided a means to directly evaluate how the increase in stiffness affected calcium signaling in the hCASMC (Figure 4A). Figure 4B provides an image of Fluo-4-labeled hCASMC in hydrogels without any magnetic particles as a negative control, whereas Figure 4C shows an image of hCASMC in MP-seeded collagen hydrogels. Averaged calcium transients indicate no significant difference in cells when the field is applied compared to no magnetic field (Figure 4D). Quantification of the rate of calcium influx also indicated no significant effect caused by the magnetic field in the absence of MPs as a function of time (Figure 4E) and averaged over all measured transients with and without the field (Figure 4F). The magnetic field also did not appear to alter the frequency of spontaneous calcium transients in the cells embedded in the non-MP-seeded collagen gels. Figure 4G shows that the application of a magnetic field significantly altered the dynamics of calcium transients of hCASMC in MR-hydrogels. The period of the transient was significantly shorter and the rate of initial influx was significantly higher. Quantification of the slope of the transient indicated that the SMCs increased their rate of calcium influx in response to the higher storage modulus yielded by the application of a magnetic field, but there was no difference between the slope of the transient between the first and last three minutes (Figure 4H). Two-sample t-tests between the "on" and "off" condition revealed a significant difference in the slope of the transient in MR hydrogels (Figure 4I). These measurements can be compared to previous studies using smooth muscle cells[35] and cardiomyocytes on 2D substrates with tunable stiffness[36] and myofibroblasts in collagen gels of differing concentrations[27], though these experiments were performed under conditions where the time scale for the response to dynamic changes to stiffness could not be measured. In contrast, the results in Figure 4 are measured after dynamically and reversibly altering stiffness on a second time scale without any alteration to the pore size of the collagen fibrous matrix. Taken together, these findings provide new insight into the effect of ECM stiffness on calcium handling in cells in 3D, and pave the way for future mechanotransduction experiments to interrogate the mechanisms by which cells respond to dynamically altered ECM mechanics.

3.7. Cell morphology in response to hydrogel stiffness in 3D

Having demonstrated the short-term, immediate cell response to changing substrate mechanics, experiments were then conducted to assess long-term changes in cell behavior. For these experiments, normal human astrocytes (NHA) were used to demonstrate the flexibility of the approach. Cells were seeded at a density of 1×10^6 cells/mL into 5 mg/mL collagen hydrogels containing 5 wt% of MPs. Rheological testing indicated that a magnetic field of 7,700 Oe increased the hydrogel stiffness from 0.8 kPa to 8.5 kPa (Figure S7), which represented a sufficient increase to investigate changes in cell morphology. Furthermore, 5 wt% MPs was chosen due to the high viability of cells seeded in hydrogels containing that concentration of MPs (Figure S8). Three conditions were tested: a magnetic field applied to the cell-seeded hydrogel in the absence of MPs (Figure 5A), cell-seeded hydrogels containing MPs in the absence of a magnetic field (Figure 5B), and cell-seeded hydrogels containing MPs and exposed to the 10,000 Oe magnetic field (Figure 5C). Cell morphology was measured at 11 and 22 hours by fixing the cells and staining with DAPI and phalloidin.

At 11 hours, the spread area of the cells in hydrogels containing the MPs and exposed to the magnetic field was significantly reduced, and the cell shape index was significantly increased compared to the other conditions (Figures 5D,E). Moreover, the cells in MP-seeded hydrogels exposed to the magnetic field continued to exhibit reduced spread area and increased cell shape index (Figures 5F-I). These findings are consistent with previous studies in 3D hydrogels showing that one phase, non-degradable hydrogels with high stiffness reduce cell spreading due to the inability of cells to elastically deform/mechanically remodel the ECM in 3D[28,37]. Although the mechanical properties of these synthetic hydrogels have exhibited a capacity to study mechanotransduction, the photo-active dynamics affect the hydrogel's pore sizes. Previous studies have shown that the stiffening effect in photocrosslinkable hydrogels resulted in a decrease of dextran diffusivity[38], limiting the ability to dynamically tune substrate stiffness without altering porosity. The cells in the hydrogels seeded with MPs and exposed to a magnetic field sense a substantially increased substrate stiffness, even though the hydrogel composition and pore size is unaffected by the presence of MPs and magnetic field.

3.8. Dynamic tuning of hydrogel mechanics to control cell mechanotransduction

Altering hydrogel mechanics with magnetic fields yields a useful tool to study cell mechanics in 3D environments, but the reversibility of the effect substantially amplifies its impact. These studies interrogated whether tuning hydrogel mechanics with transient application of a magnetic field (Figure 6A-B) could control mechanosensing by the astrocytes. Three different conditions in MP-seeded hydrogels were evaluated: (i) NHA were allowed to spread in the absence of a magnetic field for a full 22-hr period, ("off-off"), (ii) a magnetic field was applied for the first 11-hrs and then removed for the remaining time ("on-off"), and (iii) NHA experienced 11-hrs in the absence of a field and then a magnetic field was applied for the remaining 11-hrs ("off-on"). Figures 6A-C provide schematics summarizing these conditions. At the end of the 22-hr period, all hydrogels were fixed and stained with DAPI, phalloidin, and an anti-YAP antibody, given previous findings that substrate mechanics affects translocation of the transcription factor to the nucleus[4]. As Figure 6D,E show, astrocytes in the "off-off" and "on-off" conditions spread and YAP was diffuse throughout the cytoplasm. In contrast to the previous conditions, cells exposed to the "off-on" regimen exhibited increased YAP staining within the cell nucleus (Figure 6F). The was no significant difference in either the spread area or the cell shape index between the "off-on" and "on-off" conditions, though both were significantly different from the "off-off" control (Figure 6G,H). Quantification of the YAP staining verified that the "off-on" condition exhibited significantly increased nuclear translocation in Figure 6I. These results suggest that cells in the "off-on" condition initially sense a more compliant ECM and begin to spread, but once the magnetic field is applied the cells sense a stiffer environment and YAP translocation increases. In contrast, cells in the "on-off" condition are initially constrained from spreading by the increased stiffness, but once the magnetic field is removed the cells sense a softer environment and begin to spread and reduce YAP translocation. These results mirror the findings in other approaches to dynamically tune substrate stiffness with more complex alterations to hydrogel properties[10,28,37,39]. Yet, this approach requires no alteration to hydrogel composition or chemistry to dynamically tune hydrogel mechanics and interrogate cell mechanotransduction.

4. Discussion

The results presented here demonstrate that magnetic tuning of hydrogel mechanics yields a new means to study cell mechanobiology in 3D environments. One of the advantages of using MPs to dynamically alter 3D hydrogel mechanics is the ability to generalize this approach across multiple hydrogel systems and platforms. Several recent studies have examined the magnetorheological properties of MPs embedded in various hydrogels including carrageenan[17,40], alginate[41] and acrylamide[20]. Here, we demonstrate that the stiffness of several different hydrogel formulations (collagen, fibrin, collagen-hyaluronan) compatible with multiple different cell types (smooth muscle cells and astrocytes) can be altered without any modification to crosslinking chemistry or ligand density. Therefore, researchers using in vitro systems to study cell mechanobiology in 3D geometries can use MPs to dynamically alter ECM mechanics by the simple application of a magnetic field. Showing that the magnetic field does not cause measurable displacement of the MPs after gel polymerization suggests that the pore size and microstructure of the hydrogel is not altered, indicating that the magnetic field changes hydrogel mechanics independent of any effect on ligand density or topology. Therefore, magnetically active hydrogels can complement the complex light- and pH-sensitive approaches that have been used previously[12,13,28], which all require specific chemistries and substrates, providing a broadly adaptable alternative[42,43]. The results presented here mirror several results from studies using photo-crosslinkable chemistries, specifically the inability of cells to spread within hydrogels exhibiting storage moduli that exceed 10 kPa[12,28]. But they also demonstrate the potential for magnetically tunable hydrogels to provide new insight into the dynamics of cell mechanotransduction, showing that cells allowed to spread in a lower stiffness environment increase their nuclear translocation of YAP as the hydrogel becomes stiffer and instantaneous alteration of ECM mechanics results in immediate changes to calcium handling within cells in 3D.

The near-instantaneous effect of magnetic stiffening and its rapid reversibility distinguish this approach from previous means of dynamically altering 3D substrate mechanics. As shown in the rheological tests, removal of the magnetic field returns the hydrogel to its original mechanical properties nearly instantaneously. The analytical model and confocal microscopy experiments provide some insight into the mechanisms underlying these effects. In the presence of a magnetic field, the MPs likely form dipoles that resist any motion relative to adjacent particles. The application of an external mechanical stimulus causes the ferromagnetic particles to become misaligned and results in antisymmetric stresses, and thus contributes to the increase of shear modulus as demonstrated in rheological studies. Due to the stiffening effect, this resistance gives rise to the increase in hydrogel stiffness in the presence of the magnetic field, and also explains how removal of the magnetic field returns the fibrous networks to their original state. Previous studies that have demonstrated the concentration of carbonyl iron MPs substantially affect the stiffness of the hydrogel conclude that particle dispersibility contributes to a drastic change in elastic modulus compared to highly organized magnetic chains[17,18], which supports this proposed mechanism. The rheological data and live cell experiments, which represent the global and local application of force respectively, both demonstrate that MP displacement is impeded in

the presence of magnetic fields and subsequently stiffen the fibrous network. Thus, removing the magnetic field abruptly ends the stiffening effect, yielding a means to transiently and reversibly alter hydrogel mechanics.

The rapid and reversible nature of magnetic stiffening provides new insight into both short-term and chronic characteristics of the cell response. As evidenced by the calcium transient studies, smooth muscle cells respond to the stiffness of the surrounding matrix within seconds by altering the rate of calcium influx and period of the calcium transient. The MR hydrogels therefore provide a platform for future studies to interrogate the underlying molecular mechanisms by which cells sense the mechanics of their environment and alter calcium handling and actomyosin force generation within very short time scales. The morphology and YAP measurements in astrocytes also demonstrate how this technique can be used to study longer term aspects of the cell response. A previous study has shown that cells readily uptake magnetic microparticles with diameters as large as 5.8 μm without affecting cell function[44]. Therefore, the effect of dynamic stiffness on gene expression can be evaluated by probing the transcriptional state of the cells in hydrogels undergoing controlled changes in rheological properties. In this way, magnetic hydrogels provide a new means to study cell-ECM interactions in the context of various tissues. There are several physiological and pathological processes involving time-dependent changes to ECM mechanics that can be mimicked by dynamic and reversible modification of hydrogel stiffness: cardiac fibrosis[36,45,46], wound healing[47,48], tumor metastasis[49,50], and atherosclerosis[51,52] are all relevant examples. Beyond the time-dependent studies presented here, focusing of magnetic fields within sub-millimeter loci can create well-defined spatial gradients. Therefore, MP-seeded hydrogels can interrogate the effects of local stiffening within 3D in vitro blood vessel models and other microfluidic applications.

There is also the potential to use protein-based MR hydrogels in applications related to tissue engineering, given the cytocompatibility of the MPs[16,20] and the ability of magnetic fields to penetrate further into tissue than the UV light used for photocrosslinkable chemistries[53–55]. There is specific relevance for central nervous system (CNS) injury, given the results related to controlling astrocyte morphology and YAP translocation to the nucleus. Previous studies have found glial scars that form in the aftermath of CNS injury exhibit a lower stiffness than surrounding tissue, which may affect neuroregeneration[56]. Implanting hydrogels seeded with MPs into the cord provides a means to dynamically alter the stiffness of the scaffold during the healing process to encourage axon infiltration and outgrowth from the injury area. Due to the presence of the skull and spine, the CNS is also a good example of a tissue that would not be compatible with UV-photocrosslinkable means of tuning scaffold mechanical properties[55]. Overall, the flexibility of magnetic hydrogels amplifies its potential use for both in vitro and in vivo applications.

5. Conclusion

The results presented here demonstrate that a broad variety of hydrogels embedded with magnetic particles respond rapidly and reversibly to external magnetic fields. An analytical model accounting for volume-distributed torques by the magnetic particles in the presence of an external magnetic field predicts the observed increase in hydrogel storage modulus. Using

fluorescently labeled magnetic particles, we validate the model's assumption that the magnetic field does not induce substantial displacement of particles within the hydrogel. Rather, the magnetic field impedes magnetic particle displacement during both global strain of the fibrous network in a rheometer and local strain caused by cell-mediated contraction, giving rise to the observed changes in hydrogel mechanics. The results indicate that cells directly respond to changes in the hydrogel stiffness, as indicated by calcium handling in short-term experiments and cell morphology and YAP translocation during extended studies. Overall, this work establishes a new approach to interrogating cell mechanobiology in 3D without altering hydrogel microstructure and pore size.

Supplementary Material

Refer to Web version on PubMed Central for supplementary material.

Acknowledgements

This work was supported by funding from the National Science Foundation (CMMI-1728239 (PG), DMR-1720530 (EK), and CMMI-154857 (AC, AB, XC)), the Craig H. Neilsen Foundation (PG), the National Institutes of Health (GM136259 & EB017753 (PJ)), and the National Science Center, Poland, under grant number UMO-2017/26/D/ST4/0099 (KP). The authors would also like to thank William G. Marshall for his assistance with the schematics in Figures 4–6.

References

(1). Fu J; Wang YK; Yang MT; Desai RA; Yu X; Liu Z; Chen CS Mechanical Regulation of Cell Function with Geometrically Modulated Elastomeric Substrates. Nat. Methods 2010, 7 (9), 733–736. 10.1038/nmeth.1487. [PubMed: 20676108]

(2). Baker BM; Chen CS Deconstructing the Third Dimension-How 3D Culture Microenvironments Alter Cellular Cues. J. Cell Sci 2012, 125 (13), 3015–3024. 10.1242/jcs.079509. [PubMed: 22797912]

(3). Wen JH; Vincent LG; Fuhrmann A; Choi YS; Hribar KC; Taylor-Weiner H; Chen S; Engler AJ Interplay of Matrix Stiffness and Protein Tethering in Stem Cell Differentiation. Nat. Mater 2014, 13 (10), 979–987. 10.1038/nmat4051. [PubMed: 25108614]

(4). Dupont S; Morsut L; Aragona M; Enzo E; Giulitti S; Cordenonsi M; Zanconato F; Le Digabel J; Forcato M; Bicciato S; Elvassore N; Piccolo S. Role of YAP/TAZ in Mechanotransduction. Nature 2011, 474 (7350), 179–184. 10.1038/nature10137. [PubMed: 21654799]

(5). McBeath R; Pirone DM; Nelson CM; Bhadriraju K; Chen CS Cell Shape, Cytoskeletal Tension, and RhoA Regulate Stem Cell Lineage Commitment. Dev. Cell 2004, 6 (4), 483–495. 10.1016/S1534-5807(04)00075-9. [PubMed: 15068789]

(6). Hong H; Stegemann JP 2D and 3D Collagen and Fibrin Biopolymers Promote Specific ECM and Integrin Gene Expression by Vascular Smooth Muscle Cells. J. Biomater. Sci. Polym. Ed 2008, 19 (10), 1279–1293. 10.1163/156856208786052380. [PubMed: 18854122]

(7). Stegemann JP; Nerem RM Altered Response of Vascular Smooth Muscle Cells to Exogenous Biochemical Stimulation in Two- and Three-Dimensional Culture. Exp. Cell Res 2003, 283 (2), 146–155. 10.1016/S0014-4827(02)00041-1. [PubMed: 12581735]

(8). Nam S; Lee J; Brownfield DG; Chaudhuri O. Viscoplasticity Enables Mechanical Remodeling of Matrix by Cells. Biophys. J 2016, 111 (10), 2296–2308. 10.1016/j.bpj.2016.10.002. [PubMed: 27851951]

(9). Chaudhuri O. Viscoelastic Hydrogels for 3D Cell Culture. Biomater. Sci 2017, 5 (8), 1480–1490. 10.1039/c7bm00261k. [PubMed: 28584885]

(10). Chaudhuri O; Gu L; Darnell M; Klumpers D; Bencherif SA; Weaver JC; Huebsch N; Mooney DJ Substrate Stress Relaxation Regulates Cell Spreading. Nat. Commun 2015, 6, 1–7. 10.1038/ncomms7365.

(11). Das RK; Gocheva V; Hammink R; Zouani OF; Rowan AE Stress-Stiffening-Mediated Stem-Cell Commitment Switch in Soft Responsive Hydrogels. Nat. Mater 2016, 15 (3), 318–325. 10.1038/nmat4483. [PubMed: 26618883]

(12). Khetan S; Guvendiren M; Legant WR; Cohen DM; Chen CS; Burdick JA Degradation-Mediated Cellular Traction Directs Stem Cell Fate in Covalently Crosslinked Three-Dimensional Hydrogels. Nat. Mater 2013, 12 (5), 458–465. 10.1038/nmat3586. [PubMed: 23524375]

(13). Stowers RS; Allen SC; Suggs LJ; Anseth KS Dynamic Phototuning of 3D Hydrogel Stiffness. Proc. Natl. Acad. Sci. U. S. A 2015, 112 (7), 1953–1958. 10.1073/pnas.1421897112. [PubMed: 25646417]

(14). Rosales AM; Vega SL; DelRio FW; Burdick JA; Anseth KS Hydrogels with Reversible Mechanics to Probe Dynamic Cell Microenvironments. Angew. Chemie - Int. Ed 2017, 56 (40), 12132–12136. 10.1002/anie.201705684.

(15). Yang C; Tibbitt MW; Basta L; Anseth KS Mechanical Memory and Dosing Influence Stem Cell Fate. Nat. Mater 2014, 13 (6), 645–652. 10.1038/nmat3889. [PubMed: 24633344]

(16). Abdeen AA; Lee J; Bharadwaj NA; Ewoldt RH; Kilian KA Temporal Modulation of Stem Cell Activity Using Magnetoactive Hydrogels. Adv. Healthc. Mater 2016, 5 (19), 2536–2544. 10.1002/adhm.201600349. [PubMed: 27276521]

(17). Mitsumata T; Honda A; Kanazawa H; Kawai M. Magnetically Tunable Elasticity for Magnetic Hydrogels Consisting of Carrageenan and Carbonyl Iron Particles. J. Phys. Chem. B 2012, 116 (40), 12341–12348. 10.1021/jp3049372. [PubMed: 22974066]

(18). Bonhome-Espinosa AB; Campos F; Rodriguez IA; Carriel V; Marins JA; Zubarev A; Duran JDG; Lopez-Lopez MT Effect of Particle Concentration on the Microstructural and Macromechanical Properties of Biocompatible Magnetic Hydrogels. Soft Matter 2017, 13 (16), 2928–2941. 10.1039/c7sm00388a. [PubMed: 28357436]

(19). Popa EG; Santo VE; Rodrigues MT; Gomes ME Magnetically-Responsive Hydrogels for Modulation of Chondrogenic Commitment of Human Adipose-Derived Stem Cells. Polymers (Basel). 2016, 8 (2). 10.3390/polym8020028.

(20). Lee JH; Han WJ; Jang HS; Choi HJ Highly Tough, Biocompatible, and Magneto-Responsive Fe3O4/Laponite/PDMAAm Nanocomposite Hydrogels. Sci. Rep 2019, 9 (1), 1–13. 10.1038/s41598-019-51555-5. [PubMed: 30626917]

(21). Partyka PP; Godsey GA; Galie JR; Kosciuk MC; Acharya NK; Nagele RG; Galie PA Mechanical Stress Regulates Transport in a Compliant 3D Model of the Blood-Brain Barrier. Biomaterials 2017, 115, 30–39. 10.1016/j.biomaterials.2016.11.012. [PubMed: 27886553]

(22). Bowers HC; Fiori ML; Khadela JB; Janmey PA; Galie PA Cell-Matrix Tension Contributes to Hypoxia in Astrocyte-Seeded Viscoelastic Hydrogels Composed of Collagen and Hyaluronan. Exp. Cell Res 2019, 376 (1), 49–57. 10.1016/j.yexcr.2019.01.012. [PubMed: 30658092]

(23). Placone AL; McGuiggan PM; Bergles DE; Guerrero-Cazares H; Quiñones-Hinojosa A; Searson PC Human Astrocytes Develop Physiological Morphology and Remain Quiescent in a Novel 3D Matrix. Biomaterials 2015, 42, 134–143. 10.1016/j.biomaterials.2014.11.046. [PubMed: 25542801]

(24). Galie PA; Nguyen D-HT; Choi CK; Cohen DM; Janmey PA; Chen CS Fluid Shear Stress Threshold Regulates Angiogenic Sprouting. Proc. Natl. Acad. Sci 2014, 111 (22), 7968–7973. 10.1073/pnas.1310842111. [PubMed: 24843171]

(25). Tran KA; Partyka PP; Jin Y; Bouyer J; Fischer I; Galie PA Vascularization of Self-Assembled Peptide Scaffolds for Spinal Cord Injury Repair. Acta Biomater. 2020, 104, 76–84. 10.1016/j.actbio.2019.12.033. [PubMed: 31904559]

(26). Bouhrira N; Deore BJ; Sazer DW; Chiaradia Z; Miller JS; Galie PA Disturbed Flow Disrupts the Blood-Brain Barrier in a 3D Bifurcation Model. Biofabrication 2020, 12 (2). 10.1088/1758-5090/ab5898.

(27). Godbout C; Follonier Castella L; Smith EA; Talele N; Chow ML; Garonna A; Hinz B. The Mechanical Environment Modulates Intracellular Calcium Oscillation Activities of Myofibroblasts. PLoS One 2013, 8 (5). 10.1371/journal.pone.0064560.

(28). Caliari SR; Vega SL; Kwon M; Soulas EM; Burdick JA Dimensionality and Spreading Influence MSC YAP/TAZ Signaling in Hydrogel Environments. Biomaterials 2016, 103, 314–323. 10.1016/j.biomaterials.2016.06.061. [PubMed: 27429252]

(29). Shiga T; Okada A; Kurauchi T. Magnetroviscoelastic Behavior of Composite Gels. J. Appl. Polym. Sci 1995, 58 (4), 787–792. 10.1002/app.1995.070580411.

(30). Yangguang Xu GL and T. L. Magneto-Sensitive Smart Materials and Magnetorheological Mechanism. IntechOpen,. DOI: 10.5772/intechopen.84742.

(31). Landau LD; Pitaevskii LP; Lifshitz EM Electrodynamics of Continuous Media; 1984; Vol. 29. 10.1119/1.1937882.

(32). Shkel YM; Klingenberg DJ Electrostriction of Polarizable Materials: Comparison of Models with Experimental Data. J. Appl. Phys 1998, 83 (12), 7834–7843. 10.1063/1.367958.

(33). Basu A; Wen Q; Mao X; Lubensky TC; Janmey PA; Yodh AG Nonaffine Displacements in Flexible Polymer Networks. Macromolecules 2011, 44 (6), 1671–1679. 10.1021/ma1026803.

(34). Wen Q; Basu A; Winer JP; Yodh A; Janmey PA Local and Global Deformations in a Strain-Stiffening Fibrin Gel. New J. Phys 2007, 9. 10.1088/1367-2630/9/11/428.

(35). Shkumatov A; Thompson M; Choi KM; Sicard D; Baek K; Kim DH; Tschumperlin DJ; Prakash YS; Kong H. Matrix Stiffness-Modulated Proliferation and Secretory Function of the Airway Smooth Muscle Cells. Am. J. Physiol. - Lung Cell. Mol. Physiol 2015, 308 (11), L1125–L1135. 10.1152/ajplung.00154.2014. [PubMed: 25724668]

(36). Galie PA; Khalid N; Carnahan KE; Westfall MV; Stegemann JP Substrate Stiffness Affects Sarcomere and Costamere Structure and Electrophysiological Function of Isolated Adult Cardiomyocytes. Cardiovasc. Pathol 2013, 22 (3), 219–227. 10.1016/j.carpath.2012.10.003. [PubMed: 23266222]

(37). Chaudhuri O; Gu L; Klumpers D; Darnell M; Bencherif SA; Weaver JC; Huebsch N; Lee HP; Lippens E; Duda GN; Mooney DJ Hydrogels with Tunable Stress Relaxation Regulate Stem Cell Fate and Activity. Nat. Mater 2016, 15 (3), 326–334. 10.1038/nmat4489. [PubMed: 26618884]

(38). Bian L; Hou C; Tous E; Rai R; Mauck RL; Burdick JA The Influence of Hyaluronic Acid Hydrogel Crosslinking Density and Macromolecular Diffusivity on Human MSC Chondrogenesis and Hypertrophy. Biomaterials 2013, 34 (2), 413–421. 10.1016/j.biomaterials.2012.09.052. [PubMed: 23084553]

(39). Wang M; Cui C; Ibrahim MM; Han B; Li Q; Pacifici M; Lawrence JTR; Han L; Han LH Regulating Mechanotransduction in Three Dimensions Using Sub-Cellular Scale, Crosslinkable Fibers of Controlled Diameter, Stiffness, and Alignment. Adv. Funct. Mater 2019, 29 (18), 1–11. 10.1002/adfm.201808967.

(40). Ikeda J; Takahashi D; Watanabe M; Kawai M; Mitsumata T. Particle Size in Secondary Particle and Magnetic Response for Carrageenan Magnetic Hydrogels. Gels 2019, 5 (3), 1–9. 10.3390/gels5030039.

(41). Gila-Vilchez C; Duran JDG; Gonzalez-Caballero F; Zubarev A; Lopez-Lopez MT Magnetorheology of Alginate Ferrogels. Smart Mater. Struct 2019, 28 (3). 10.1088/1361-665X/aafeac.

(42). Binder WH; Sachsenhofer R. “Click” Chemistry in Polymer and Materials Science. Macromol. Rapid Commun 2007, 28 (1), 15–54. 10.1002/marc.200600625.

(43). Hoyle CE; Bowman CN Thiol-Ene Click Chemistry. Angew. Chemie - Int. Ed 2010, 49 (9), 1540–1573. 10.1002/anie.200903924.

(44). Shapiro EM; Sharer K; Skrtic S; Koretsky AP In Vivo Detection of Single Cells by MRI. Magn. Reson. Med 2006, 55 (2), 242–249. 10.1002/mrm.20718. [PubMed: 16416426]

(45). Suezawa C; Kusachi S; Murakami T; Toeda K; Hirohata S; Nakamura K; Yamamoto K; Koten K; Miyoshi T; Shiratori Y. Time-Dependent Changes in Plasma Osteopontin Levels in Patients with Anterior-Wall Acute Myocardial Infarction after Successful Reperfusion: Correlation with Left-Ventricular Volume and Function. J. Lab. Clin. Med 2005, 145 (1), 33–40. 10.1016/j.lab.2004.08.007. [PubMed: 15668659]

(46). Pilewski JM; Liu L; Henry AC; Knauer AV; Feghali-Bostwick CA Insulin-like Growth Factor Binding Proteins 3 and 5 Are Overexpressed in Idiopathic Pulmonary Fibrosis and Contribute to

Extracellular Matrix Deposition. Am. J. Pathol 2005, 166 (2), 399–407. 10.1016/S0002-9440(10)62263-8. [PubMed: 15681824]

(47). Genever PG; Cunliffe WJ; Wood EJ Influence of the Extracellular Matrix on Fibroblast Responsiveness to Phenytoin Using in Vitro Wound Healing Models. Br. J. Dermatol 1995, 133 (2), 231–235. 10.1111/j.1365-2133.1995.tb02620.x. [PubMed: 7547389]

(48). Tracy LE; Minasian RA; Caterson EJ Extracellular Matrix and Dermal Fibroblast Function in the Healing Wound. Adv. Wound Care 2016, 5 (3), 119–136. 10.1089/wound.2014.0561.

(49). Netti PA; Baxter LT; Boucher Y; Jain RK; Skalak R. Time-Dependent Behavior of Interstitial Fluid Pressure in Solid Tumors: Implications for Drug Delivery. Cancer Res. 1995, 55 (22), 5451–5458. [PubMed: 7585615]

(50). Yuan F; Chen Y; Dellian M; Safabakhsh N; Ferrara N; Jain RK Time-Dependent Vascular Regression and Permeability Changes in Established Human Tumor Xenografts Induced by an Anti-Vascular Endothelial Growth Factor/Vascular Permeability Factor Antibody. Proc. Natl. Acad. Sci. U. S. A 1996, 93 (25), 14765–14770. 10.1073/pnas.93.25.14765. [PubMed: 8962129]

(51). Ponticos M; Smith BD Extracellular Matrix Synthesis in Vascular Disease: Hypertension, and Atherosclerosis. J. Biomed. Res 2014, 28 (1), 25–39. 10.7555/JBR.27.20130064. [PubMed: 24474961]

(52). Spinale FG; Coker ML; Thomas CV; Walker JD; Mukherjee R; Hebbar L. Time-Dependent Changes in Matrix Metalloproteinase Activity and Expression during the Progression of Congestive Heart Failure: Relation to Ventricular and Myocyte Function. Circ. Res 1998, 82 (4), 482–495. 10.1161/01.RES.82.4.482. [PubMed: 9506709]

(53). Fleischmann EM The Measurement and Penetration of Ultraviolet Radiation into Tropical Marine Water. Limnol. Oceanogr 1989, 34 (8), 1623–1629. 10.4319/lo.1989.34.8.1623.

(54). Yasui M; Ikuta K. Modeling and Measurement of Curing Properties of Photocurable Polymer Containing Magnetic Particles and Microcapsules. Microsystems Nanoeng. 2017, 3. 10.1038/micronano.2017.35.

(55). Nakata M; Nagasaka K; Shimoda M; Takashima I; Yamamoto S. Focal Brain Lesions Induced with Ultraviolet Irradiation. Sci. Rep 2018, 8 (1), 1–11. 10.1038/s41598-018-26117-w. [PubMed: 29311619]

(56). Moeendarbary E; Weber IP; Sheridan GK; Koser DE; Soleman S; Haenzi B; Bradbury EJ; Fawcett J; Franze K. The Soft Mechanical Signature of Glial Scars in the Central Nervous System. Nat. Commun 2017, 8, 1–11. 10.1038/ncomms14787. [PubMed: 28232747]

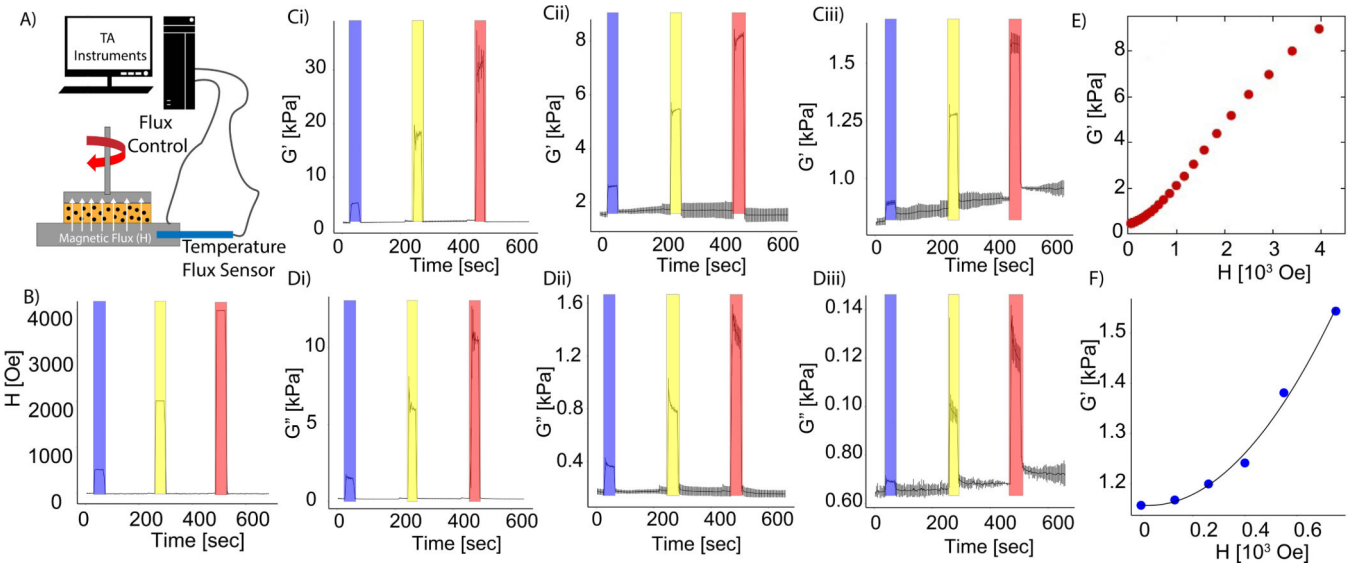

Figure 1.

Magneto-rheological characterization of common hydrogels and model validation. **(A)** Magnetorheology test set-up with axial application of magnetic field to hydrogels within a cone and plate geometry. **(B)** Variation of magnetic field controlled by the magnetorheometer. Blue = 500 Oe, yellow = 2000 Oe red = 4000 Oe. Collagen hydrogel storage moduli with **(C,i)** 10 wt%, **(C,ii)** 5 wt%, and **(C,iii)** 0.5 wt% MPs. Loss modulus of **(D,i)** 10 wt%, **(D,ii)** 5 wt%, and **(D,iii)** 0.5 wt% MPs. Data presented as mean ± s.d. (n = 3). **(E)** Dependence of 1 mg/mL fibrin storage modulus on magnetic field strength. **(F)** Measurement of PDMS storage modulus, embedded with 10 wt% MPs, as a function of magnetic field (blue circles) and prediction of analytical model (line).

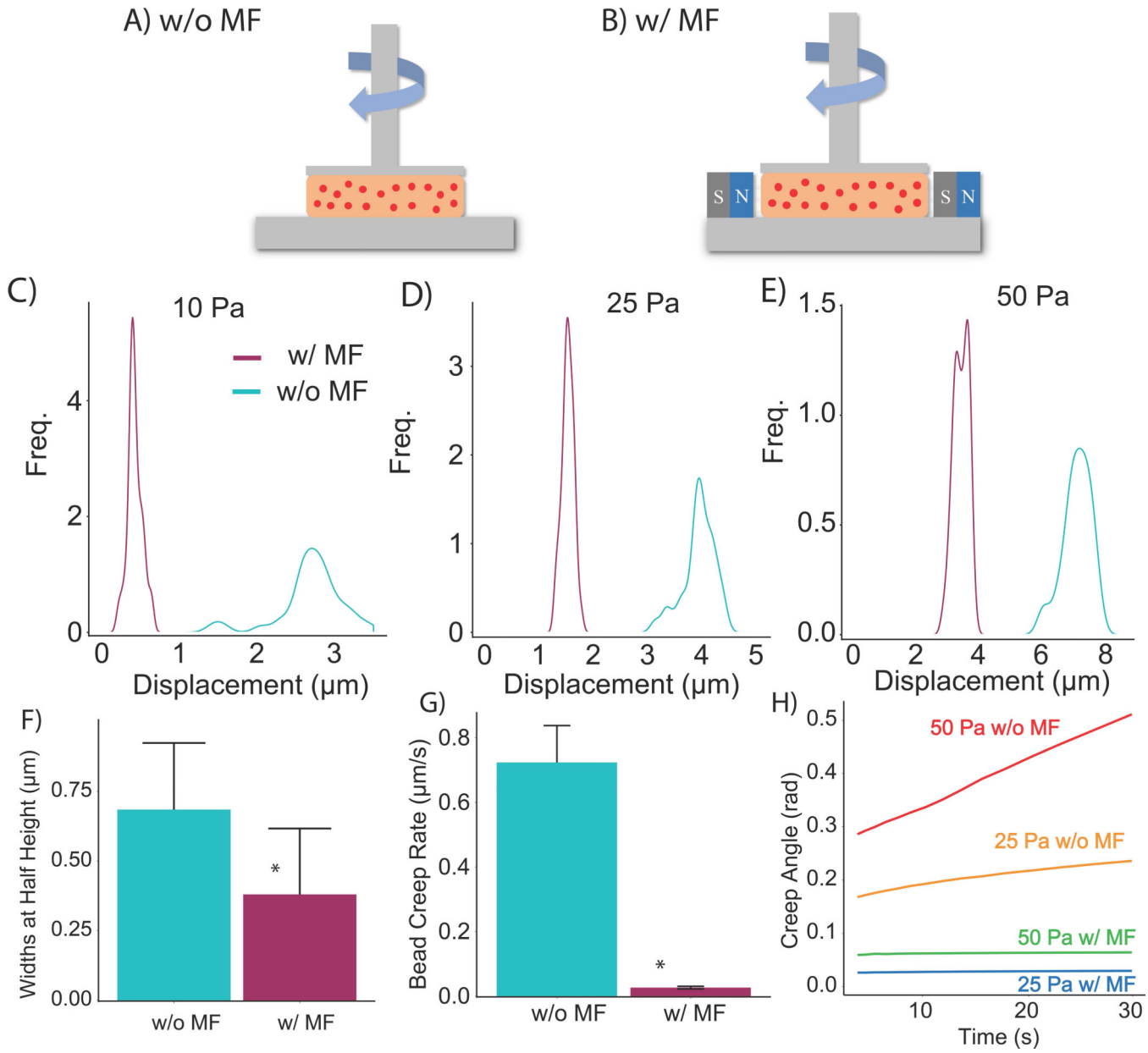

Figure 2.

Displacement of magnetic particles within 2 mg/mL and 5 mg/mL collagen hydrogels. Confocal images of 0.5 wt% magnetic particles in 2 mg/mL collagen hydrogels **(A)** prior to polymerization and **(B)** post polymerization (20-seconds between images) (n = 115). Fluorescent images of 0.5 wt% magnetic particles in 5 mg/mL collagen hydrogels **(C)** prior to polymerization and **(D)** post polymerization, (n = 115). Cyan = without magnetic field, magenta = with magnetic field of 2500-Oe. Scale = 50-μm. **(E,F)** Quantification of bead displacement in response to a magnetic field in 2 mg/mL and 5 mg/mL collagen hydrogels. **(G)** Box plots of bead displacement. *p < 0.05

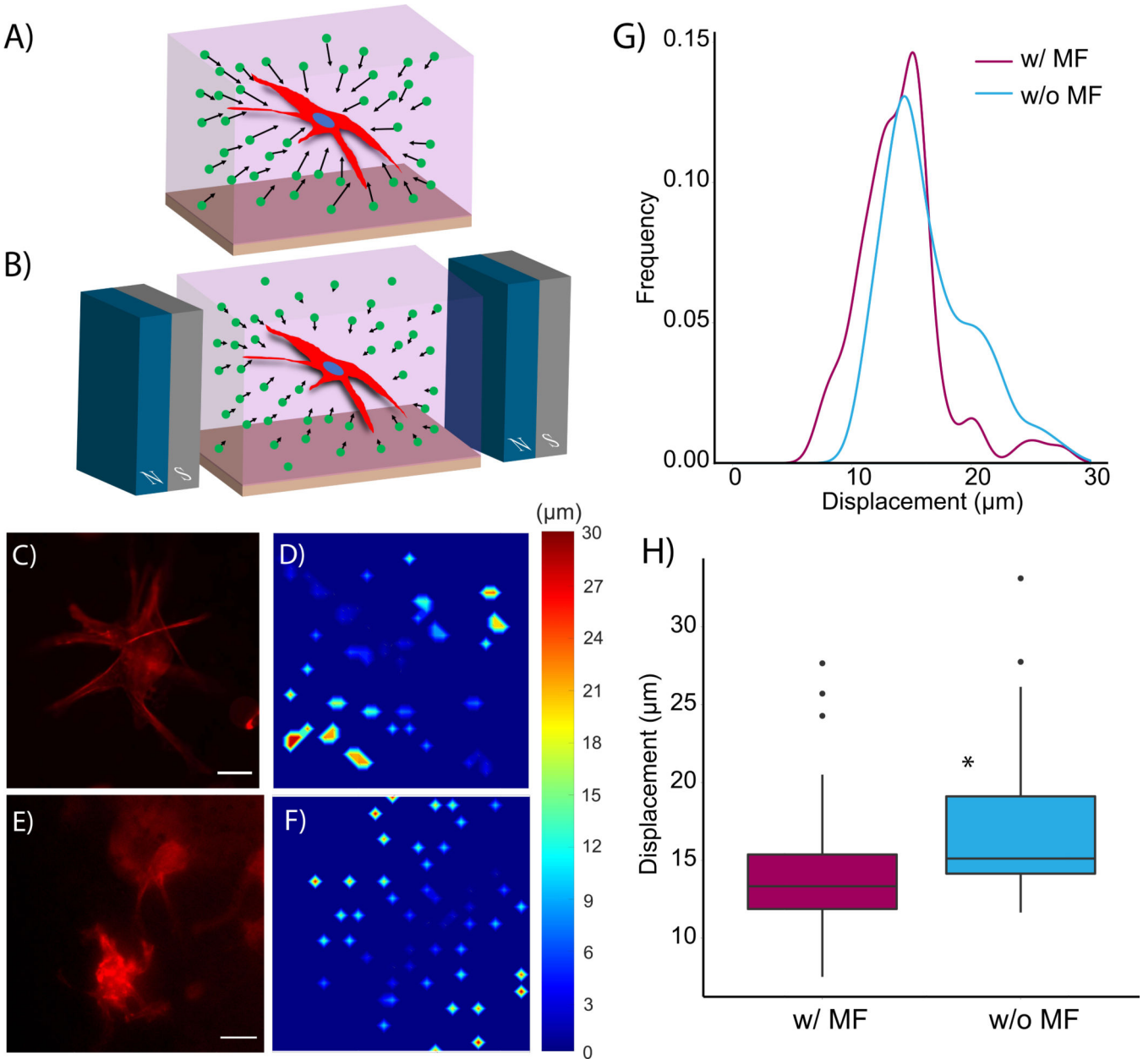

Figure 3.

Schematic of rheometer setup of magnetically responsive fibrin hydrogels **(A)** without and **(B)** with a magnetic field (MF). Quantification of instantaneous bead displacement undergoing **(C)** 10 Pa, **(D)** 25 Pa, **(E)** 50 Pa shear stress with and without 1000-Oe magnetic field (n = 35 per condition). **(F)** Average width of the instantaneous displacement distribution. **(G)** Creep rate measured by tracking bead displacement in fibrin gels exposed to 50 Pa of shear stress over 30 seconds (n = 3). **(H)** Creep angle measured from the rheometer. These fibrin hydrogels contained 1 wt% of MPs. * $p < 0.05$

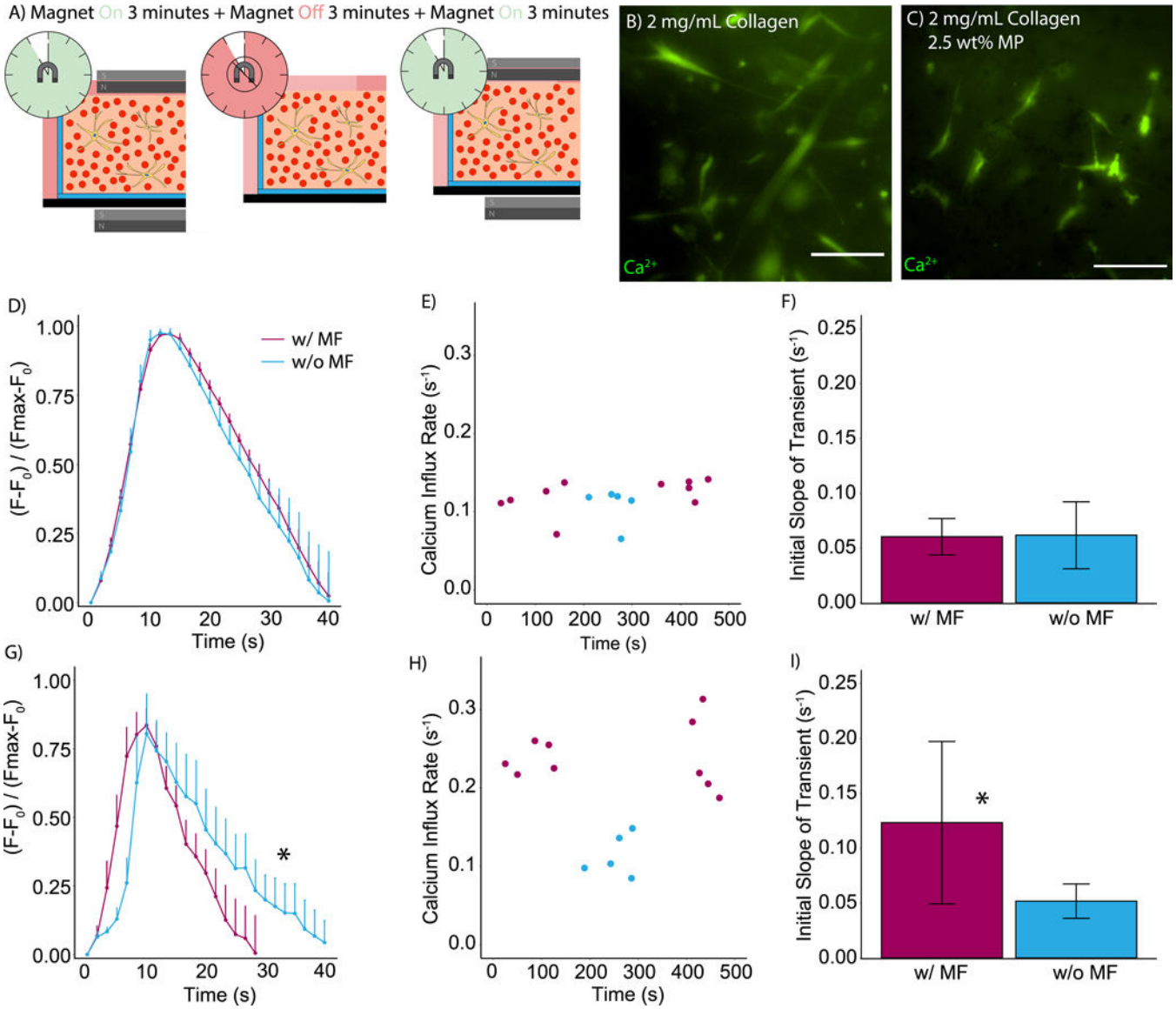

Figure 4.

Schematic of 3D hydrogels used for live cell microscopy **(A)** without and **(B)** with a 500-Oe magnetic field (MF). RFP-LifeACT-labeled hCASMC in 5 mg/mL collagen, 1 mg/mL HA, and 0.5 wt% MPs **(C)** without a magnetic field and **(D)** corresponding heat map of bead displacement. **(E)** Cells and **(F)** heat map with a magnetic field. Quantification of beads' displacement due to cell motility with **(G)** 0 Oe (w/o MF) and 500 Oe (w/ MF) (n = 75 beads per condition). Box and whisker plots of **(H)** bead displacement. Scale = 25-μm. *p < 0.05.

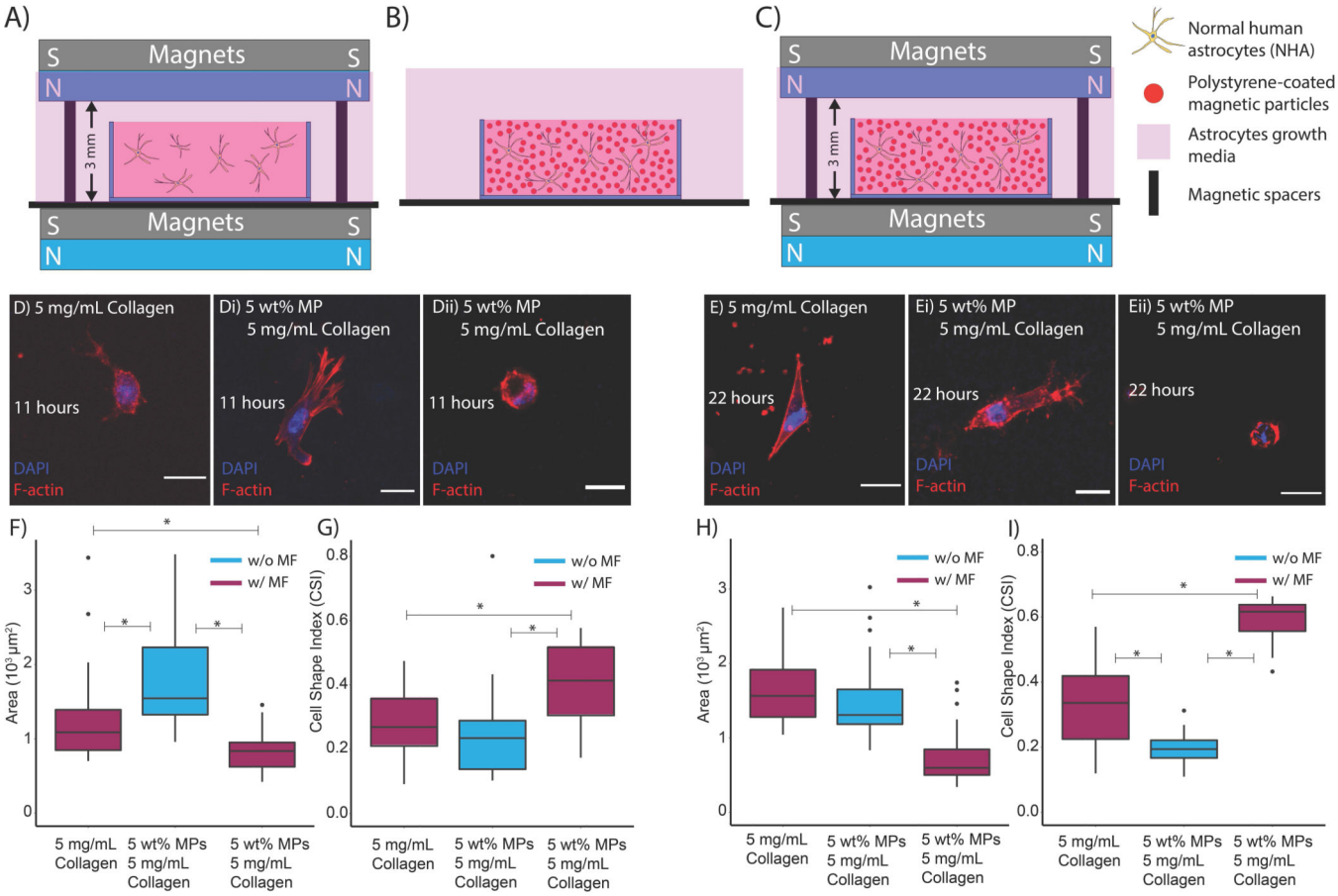

Figure 5.

Schematic of cell experiments with **(A)** 5 mg/mL collagen in the presence of a 10,000 Oe magnetic field, **(B)** 5 mg/mL collagen and 5 wt% magnetic particles (MPs) without a magnetic field, and **(C)** 5 mg/mL collagen and 5 wt% magnetic particles (MPs) with a 10,000-Oe field. Representative images of cells in **(D)** for the three conditions at 11 hours. Representative images of cells in **(E)** for the three conditions at 22 hours. Quantification of **(F)** cell area and **(G)** cell shape index (CSI) for the 11-hour timepoint and **(H)** cell area and **(I)** cell shape index (CSI) for the 22-hour timepoint. DAPI (blue) and F-actin (red). Scale = 25-µm. *p <0.05. (n > 25 per condition)

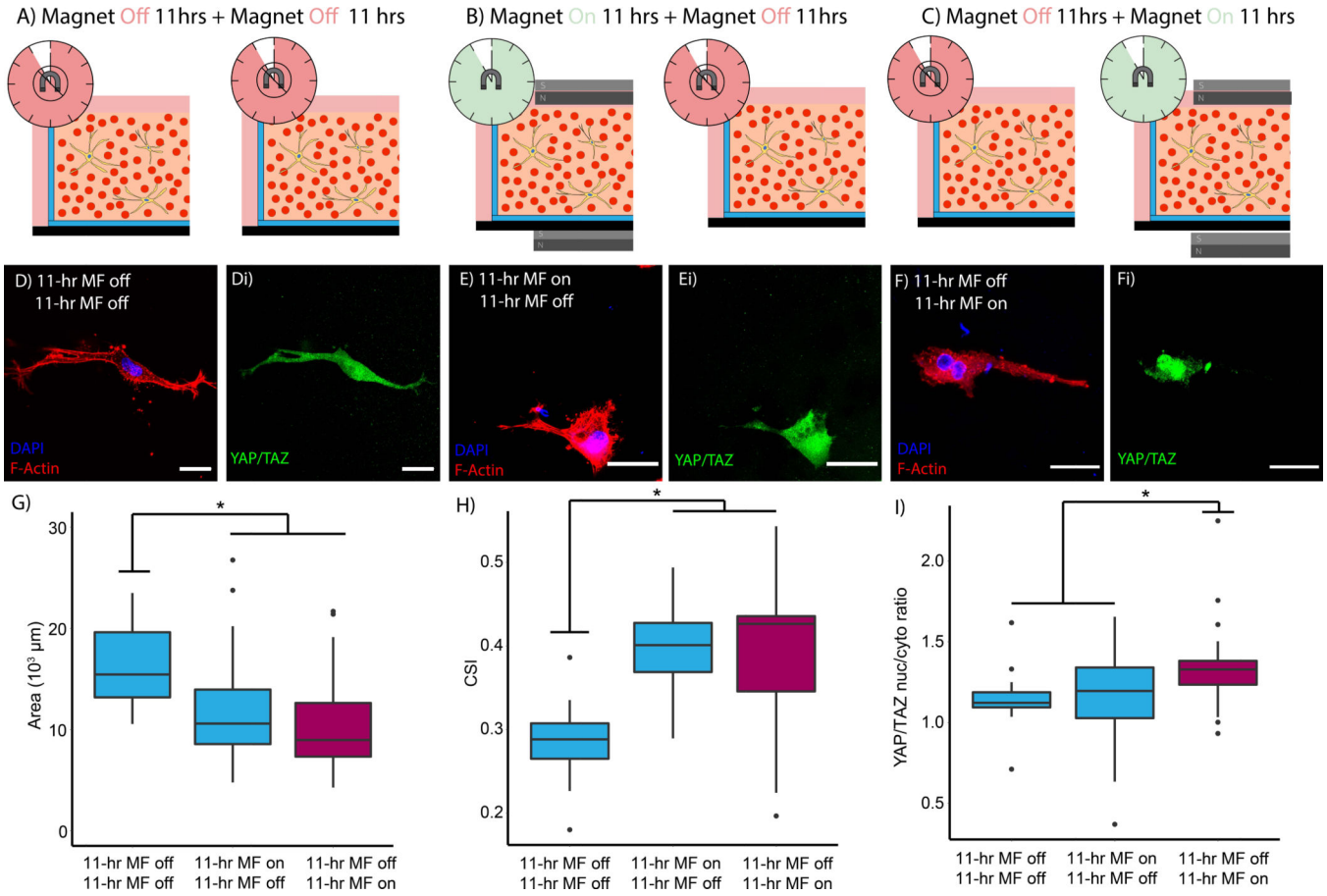

Figure 6.

Dynamically tunable hydrogels by transient application of a 10,000-Oe magnetic field **(A,B)**. Representative images of **(C)** cell morphology and **(Ci)** YAP in the “off-on” condition. Representative images of **(D)** cell spreading and **(Di)** YAP in the “on-off” condition. Quantification of **(E)** cell area, **(F)** cell shape index, and **(G)** nuclear to cytoplasmic YAP ratio. DAPI (blue), F-actin (red), and YAP (green). Scale = 25-µm. *P < 0.05. (n > 25 cells per condition).